IEEE Access
Multidisciplinary ⋮ Rapid Review ⋮ Open Access Journal

Received December 10, 2019, accepted January 4, 2020, date of publication January 9, 2020, date of current version January 17, 2020.

Digital Object Identifier 10.1109/ACCESS.2020.2965209

Adapting of Non-Metallic Cookware for Induction Heating Technology via Thin-Layer Non-Magnetic Conductive Coatings

J. ACERO[1], (Member, IEEE), I. LOPE[2,3], (Member, IEEE), C. CARRETERO[2], (Senior Member, IEEE), AND J. M. BURDIO[1], (Senior Member, IEEE)

[1]Department of Electronic Engineering and Communications, University of Zaragoza, 50018 Zaragoza, Spain
[2]Department of Applied Physics, University of Zaragoza, 50009 Zaragoza, Spain
[3]BSH Home Appliances, 50016 Zaragoza, Spain

Corresponding author: J. Acero (jacero@unizar.es)

This work was supported in part by the Spanish MINECO under Project TEC2016-78358-R, in part by the Spanish MICINN and AEI under Project RTC-2017-5965-6, co-funded by EU through FEDER Program, and in part by the BSH Home Appliances Group.

ABSTRACT We analyze the feasibility of heating non-metallic cookware, unappropriate for heating by means of induced currents, with the purpose of extending the applicability range of the current induction heating cooktops. In order to turn materials as glass, ceramic, wood or plastic into suitable for the induction heating technology, we propose the use of thin layers of a metal (not necessarily a ferromagnetic material) which can be deposited on a surface by means of a thin or thick layer technology. For this purpose, the inductive performance of these layers is investigated by means of an analytical electromagnetic model, finite element simulations and experimental measurements. Calculations point out that for a specific induction arrangement working at a fixed frequency, it exists a thickness which maximizes the induction efficiency for each layer material. The suitability of this result is tested by means of a set of samples with copper thin layers whose thicknesses range from one hundred of nanometers to tens of micrometers, which are implemented using a phase vapor deposition (PVD) technology. The obtained induction efficiency and equivalent resistance are compared with those obtained with conventional ferromagnetic materials. As a proof of concept, the inner and outer bottoms of two glass pots are covered with a copper layer of 2 μm, and 1.5 μm, respectively, and 1 kW is inductively supplied by means of a series resonant inverter, reaching the boiling water conditions.

INDEX TERMS Eddy currents, energy efficiency home appliances, induction heating, impedance matching, thin layer.

I. INTRODUCTION

In the last years, the induction heating technology has progressively penetrated in the domestic sphere due to its superior advantages as CO_2-emission free heating, safety, cleanliness and high efficiency. Part of these advantages derives from the fact that the heat is directly generated in the cookware and, therefore high-temperature heat sources (as flames, or radiant heaters) which transfer a considerable part of the energy into the air, are eliminated. Other advantages of typical domestic induction heating applications derive from the implemented advanced electronics, including power converters, digital controllers and user interfaces. Among these advantages, the most popular are automatic pot detection, high output power capability, and power and temperature controllability. Despite these advantages, this technology also present some drawbacks, as the impossibility of heat non-metallic cookware made of glass, plastic or ceramics, and, the low efficiency reached with non-ferromagnetic materials [1].

In the literature many works proposing different power electronic solutions [2]–[5], modelling and digital modulation strategies [6]–[8] and improvements of the inductor system of induction cookers [9]–[14] have been reported.

The associate editor coordinating the review of this manuscript and approving it for publication was Karol Malecha.

However, advances in induction heating loads (i.e. the pots) can hardly be found. Domestic induction heating loads are mainly made of ferromagnetic steel because this material naturally provides good performance. Especially, high induction efficiency, up to 98%, can be achieved at the usual operation frequency range, from 20 to 100 kHz [15]. Nevertheless, pots made of non-ferromagnetic metals (as aluminum, copper or stainless steel) present high quality factor Q, low equivalent impedance [16] and low efficiency. Moreover, due to physical reasons, non-metallic cookware can not be heated by means of the induction mechanism. For this reason, current cooktops automatically detect and reject heating the mentioned non-ferromagnetic and non-metallic cookware. The requirement of using specific cookware is one of the most unpopular characteristics of induction cookers.

The suitability of a material for induction heating can be explained by means of its sheet resistance at a given frequency. This resistance is very high in the case of non-conductive materials (tens or hundreds of kΩ) and, therefore, in these conditions it is not possible to induce enough current to achieve a perceptible Joule heating. On the contrary, considering the properties of a typical F114 ferromagnetic steel $\left(\sigma_{\mathrm{Fe}} = 2 \times 10^6 (\Omega\mathrm{m})^{-1},\ \mu_{r,\mathrm{Fe}} = 400\right)$ and an aluminum $\left(\sigma_{\mathrm{Al}} = 3 \times 10^7 (\Omega\mathrm{m})^{-1},\ \mu_{r,\mathrm{Al}} = 1\right)$, at 100 kHz their skin depth δ are 56 μm and 290 μm, respectively. Therefore, at this frequency the sheet resistances per square (□) are $R_{\mathrm{sheet,Fe}} = 9\ \mathrm{m}\Omega/\square$ and $R_{\mathrm{sheet,Al}} = 0.11\ \mathrm{m}\Omega/\square$, respectively. Therefore, for the same induced current level the dissipation in the F114 is more than seventy five times higher than in the aluminum. This is very illustrative because the inability of heating non-ferromagnetic materials is commonly attributed to the absence of the magnetic hysteresis.

The immediate conclusion is that an optimal material for induction heating should have a balanced sheet resistance, neither too low nor too high. The sheet resistance of a workpiece can be adjusted according to two ways. First, by choosing a material with appropriate conductivity and magnetic permeability. However, in the nature the set of materials with convenient properties is small and the case of the iron is almost an exception [17]. The second possibility is to make thin layers of a good conductor, where the sheet resistance is determined by the thickness of the layer. In this case the current is forced to flow through a layer of a good conductor with small cross section. Following the precedent example, the sheet resistance of an aluminum layer of 2.3 μm is 14 mΩ. Obviously, the thickness required to achieve this sheet resistance is lower than the corresponding skin depth at a given frequency. In the past this idea was used in the industry of semiconductor manufacturing in order to selectively heat different areas of a chip, as it appears in some patents [18].

In this work, the feasibility of using thin layers of non-magnetic good conductors for induction heating applications is explored. This idea was preliminary tested in some works [19], [20], and in this case, apart from an appropriate modeling, a proof of concept consisting of heating a glass pot with a copper thin layer deposited by using a phase vapor deposition (PVD) technique is presented. This technique allows to achieve a high precision of the layer thickness. The paper is organized as follows. Section II pursues to derive an analytical solution of the simplest induction system with the objective of obtaining an electrical model of the system. This model is complemented with the FEA simulations of Section III mainly oriented to obtain the induction efficiency. Section IV presents the experimental results with a set of samples having copper layers of different thicknesses. The design, impedance measurements and results at real heating conditions of two glass pots with copper layers are presented in Section V. Finally, some conclusions are drawn in Section VI.

II. ANALYSIS AND MODELING OF AN INDUCTION SYSTEM WITH A THIN LAYER LOAD

Usually, the analysis and modeling of induction systems has been accomplished by means of finite element simulations [21], [22]. The typical dimensions of an induction application can be up to several tens of centimeters whereas the thickness of the conductive layers here proposed ranges from nanometers to microns. Therefore, the FEA simulation of these systems becomes problematic because high resolution meshes are required. This situation is similar to the case of magnetic components with litz wires, where FEA simulations capturing the structure of the windings are unfeasible [23]. In this work we follow a double analysis way: on the one hand, an analytical solution of the system (with some assumptions) is used mainly to analyze the effect of the thickness of the layer on the inductive performance; on the other hand, FEA simulations are also carried out to evaluate the induction efficiency of particular cases.

A. PARAMETERS OF STUDY

The performance of an induction heating system can be characterized by means of two parameters: the equivalent induced load resistance R_l [24], [25], and the induction efficiency η_{ind} [15]. The resistance R_l represents the power dissipated in the load by means of the induction phenomenon. The induction efficiency is the part of the power delivered into the load with respect to the electrical power supplied into the coil and usually can be represented by means of a ratio between resistances. Considering that in an induction application the power can be dissipated by the induction phenomenon in the load and other elements (as ferrites or shielding) and also is dissipated in the windings, the induction efficiency is

$$\eta_{\mathrm{ind}} = \frac{R_l}{R_{\mathrm{ind}} + R_w}, \tag{1}$$

where R_w is the resistance of the windings and R_{ind} the resistance representing all possible induction dissipations. Typically, the resistance R_{ind} includes R_l and the dissipation in ferrites and shielding. The resistance R_{ind} depends on the frequency, the number of turns of the coil, the properties of the dissipative media, and some geometrical parameters,

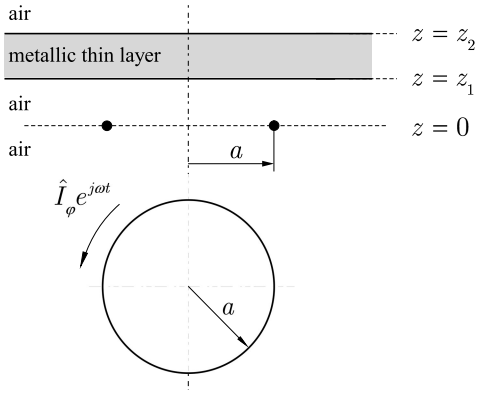

FIGURE 1. Basic induction heating system with a conductive layer.

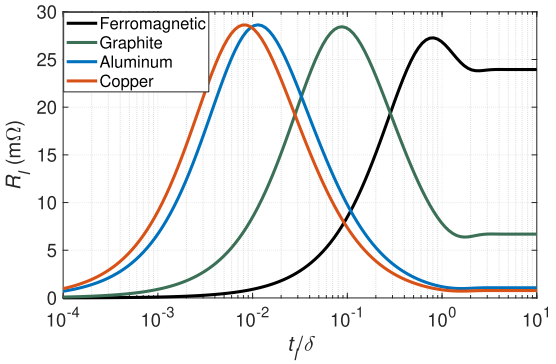

FIGURE 2. Power dissipated in the layer with respect to the ratio of the thickness to the skin depth for different materials.

as the distance between the windings an the media. The winding resistance, R_w also depends on the type of the cable.

The resistance R_l is useful for estimating the suitability of materials to be heated by means of induction, whereas η_{ind} is a Figure of Merit when design a specific induction system. In this work, R_l is calculated by means of an analytical approach whereas η_{ind} is obtained by using the finite element tool COMSOL.

B. ANALYTICAL MODEL

Fig. 1 shows the simplest induction system which can be considered for this study. This system consists of an ac filamentary current of radius a and value $\hat{I}_\varphi e^{j\omega t}$, where $\hat{I}_\varphi$ is the amplitude and ω the angular frequency, and a thin layer of a metallic material. The layer is placed at a distance $d_l = z_1$ above the filamentary current and its thickness is $t_l = z_2 - z_1$. The system is in the air and the lateral dimensions of the layer are much larger than the filamentary current radius. Assuming linear properties of the materials (electrical conductivity, magnetic permeability and permittivity) and cylindrical symmetry, a semi-analytical solution of the Maxwell's equations can be obtained [26], [27]. This solution is available for the general case of a stratified multilayer system [28], which is particularized for the case shown in Fig. 1, leading to the following expression of the impedance

$$Z_{\text{ind}} = j\omega\mu_0\pi \int_0^\infty \left[1 + \phi_{\text{eq}} e^{-2\beta z_1}\right] [aJ_1(a\beta)]^2 d\beta, \quad (2)$$

where the parameters and functions involved in this equation are explained in the next paragraph. In general this impedance is complex and therefore $Z_{\text{ind}} = R_{\text{ind}} + j\omega L_{\text{ind}}$. Taking into account the ideal (i.e. filamentary) current model of the single-turn winding, the real part of Z_{ind} represents the power dissipated in the layer or, equivalently, in this case $R_{\text{ind}} = R_l$.

In (2), $J_1(x)$ is the Bessel function of the first kind and order one, and β is the integration variable of the Fourier-Bessel transform. The function ϕ_{eq} includes the dependencies of the impedance with respect to the media properties and geometry

$$\phi_{\text{eq}}(\beta) = \frac{\left(1 - e^{-2\eta_l t_l}\right)}{\left(1 - \phi_l^2 e^{-2\eta_l t_l}\right)} \phi_l, \quad (3)$$

where

$$\phi_l(\beta) = \frac{\beta\mu_{rl} - \eta_l}{\beta\mu_{rl} + \eta_l}, \quad (4)$$

and

$$\eta_l(\beta) = \sqrt{\beta^2 + j\omega\mu_l\sigma_l}. \quad (5)$$

The preceding results can be extended to the case of multi-turn coils by replacing in (2) the term $aJ_1(a\beta)$ by $\sum_{i=1}^{n} a_i J_1(a_i\beta)$, where a_i is the radius of the i^{th} turn, and n is the number of turns. The results of the multi-turn case are equal to those obtained with a mean-length single-turn coil scaled by a n^2 factor. Ferrites, which are usually placed beneath the windings in current arrangements, enhance the results obtained with respect to the air case, but neither the essentials nor the conclusions are modified. The interest of analyzing the case shown in Fig. 1 is due to these reasons.

C. CALCULATION RESULTS

The analytical model facilitates some studies, as the effect of the thickness of the layer on the induced power, which is represented by R_l. Instead of considering the layer thickness as a study parameter, in this work is rather considered the ratio of the layer thickness to the skin depth, i.e. t_l/δ, because it allows to compare between materials of different properties. Considering the induction system shown in Fig. 1, the following parameters are defined for this study: turn radius $a = 50$ mm, distance between the turn and the layer $z_1 = 5$ mm, current amplitude $\hat{I}_\varphi = 1$ A, and frequency $f = 100$ kHz. The ratio t_l/δ ranges from 1×10^{-4} (which in some cases would correspond to a layer thickness of several nanometers) to 10. Different materials are also considered in these simulations. The simulated materials are copper $\left(\sigma_{\text{Cu}} = 5.8 \times 10^7 (\Omega\text{m})^{-1},\ \mu_{r,\text{Cu}} = 1\right)$, graphite $\left(\sigma_{\text{C}} = 5 \times 10^5 (\Omega\text{m})^{-1},\ \mu_{r,\text{C}} = 1\right)$, aluminum and ferromagnetic steel, whose properties are defined in the preceding section.

Fig. 2, shows the results of the analytical calculations. In this figure, small values of t_l/δ correspond to very thin layers, which in turn have high sheet resistance. In this case,

R_l is also very small for every material, due to the small induced power. At the other extreme, high values of t_l/δ correspond to thick layers, or in other words, corresponds to the materials in bulk. In this case, it is observed that R_l tends to a constant value when $t_l/\delta > 1$. This constant value is the expected R_l of each material in usual applications, and obviously, it its greater for ferromagnetic materials. However, as it can be observed in the middle range of t_l/δ, the value of R_l can be maximized for each material when a layer with an appropriate thickness is used. This thickness is different for each material and frequency. Regarding the definition of the induction efficiency (1), this fact represents an opportunity of maximizing the induction efficiency. As it can be also inferred, greater efficiency than the obtained with the usual ferromagnetic cookware could theoretically be reached by using appropriate layers.

It is also noticeable that the maximum values of R_l are very similar for the tested materials but at different thicknesses. This fact could mean that for a given induction heating system with fixed geometry, number of turns and frequency, the maximum R_l achievable is independent of the material, if an optimal layer is used.

III. FINITE ELEMENT MODELING AND INDUCTION EFFICIENCY

Analytical model and finite element simulation complement each other because the later allows to take into account the usual elements of induction heating appliances, as ferrites or shielding, and it also allows to obtain the induction efficiency. In any case, a useful FEA modeling also requires some simplifications and assumptions:

- Axial symmetry is assumed, therefore a 2D simulation model is developed.
- The multiturn winding made of an intricate litz wire is replaced by an ideal constant current density of rectangular cross section of area $S_{\text{coil}} = (r_{\text{ext}} - r_{\text{int}}) \cdot t_w$, where r_{int} and r_{ext} corresponds to the radii of the first and last turn, respectively, and t_w is the diameter of the cable.
- Ferrite bars are replaced by an equivalent disk.
- The thickness of the aluminum shielding usually placed beneath the ferrites is assumed greater than the skin depth at the working frequency. Therefore this element is replaced by an Impedance Boundary Condition (IBC) provided by the COMSOL tool.
- Linear properties of materials are considered. Moreover, loss free materials are also considered, except the layer and the shielding.

The schematic representation of the FEA model is shown in In Fig. 3

The winding carries a harmonic current of value $i = \text{Re}\left(\hat{I}_\varphi e^{j\omega t}\right)$. Therefore, the coil current density and voltage are

$$J = \frac{i}{S_{\text{turn}}}\hat{\boldsymbol{\varphi}} = n\frac{i}{S_{\text{coil}}}\hat{\boldsymbol{\varphi}} \tag{6}$$

$$v = -\int E \cdot dl = -\frac{n}{S_{\text{coil}}}\int_{V_{\text{coil}}} E_\varphi dv \tag{7}$$

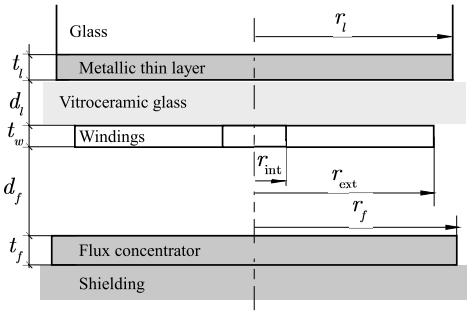

FIGURE 3. 2D FEA geometry and parameters.

where E_φ is the electrical field in the coil. An impedance of the ideal coil whose origin is the induction phenomenon is defined as $Z_{\text{ind}} = v/i$. The real part of Z_{ind} corresponds to the power dissipated in both the layer and the shielding. This power can be represented by means of two resistances (whose value can be obtained in the simulation) called R_l and R_{sh}, respectively. Therefore $R_{\text{ind}} = R_l + R_{\text{sh}}$.

Winding losses are calculated assuming litz wire windings whose strands are equivalent. In these conditions, formulas can be applied for calculating the dc, skin and proximity resistances [29], [30]. The magnetic field in the coil obtained from the FEA simulations is required for estimating the proximity losses. In this case, it is also assumed that the presence of the cable does not modify the magnetic field. Considering a cable of n_s strands of diameter $\phi_s = 2r_s$, the dc, skin and proximity resistances formulas are

$$R_{\text{dc\_skin}} = \frac{n}{n_s}\frac{\text{MLT}}{\sigma_w\left(\pi r_s^2\right)}\Phi_{\text{skin}}\left(\frac{r_s}{\delta}\right) \tag{8}$$

$$R_{\text{prox}} = n_s n\frac{4\pi}{\sigma_w}\Phi_{\text{prox}}\left(\frac{r_s}{\delta}\right)\left\langle\left|\overline{H}_t\right|^2\right\rangle_{\text{coil}} \tag{9}$$

where σ_w is electrical conductivity of the wire, δ is the skin depth at a particular frequency, MLT is the mean length of turn of the coil, $\Phi_{\text{skin}}\left(r_s/\delta\right)$, $\Phi_{\text{prox}}\left(r_s/\delta\right)$ include the ac dependency of the skin and proximity resistances of a strand per unit of length, and $\left\langle\left|\overline{H}_t\right|^2\right\rangle_{\text{coil}}$ is the average of the squared magnetic field in the coil, which can be obtained from the FEA simulation. The bar over the H_t symbol denotes the normalized magnetic field strength per unit of Amp. In these conditions, the units of $\left\langle\left|\overline{H}_t\right|^2\right\rangle_{\text{coil}}$ are $\left[\text{m}^{-1}\right]$. Usually the strand radius is chosen of the same order of magnitude of the skin depth at the design frequency, which is commonly called the low-frequency regime [31]. Under this condition, $\Phi_{\text{skin}} \approx 1$, i.e. $R_{\text{dc\_skin}}$ equals to the dc resistance of the windings, and $\Phi_{\text{prox}} \approx \frac{1}{4}\left(\frac{r_s}{\delta}\right)^4$.

An induction system comprising the inductor, the flux concentrator disk, the shielding beneath the flux concentrator, and the load is simulated. According to Fig. 3, the parameters of this system are $r_{\text{int}} = 25$ mm, $r_{\text{ext}} = 75$ mm, $t_w = 4$ mm, radius of the load $r_l = 100$ mm, distance between the winding and the load $d_l = 5$ mm, distance between the winding and the ferrite $d_f = 1$ mm, radius of the ferrite $r_f = 120$ mm, and

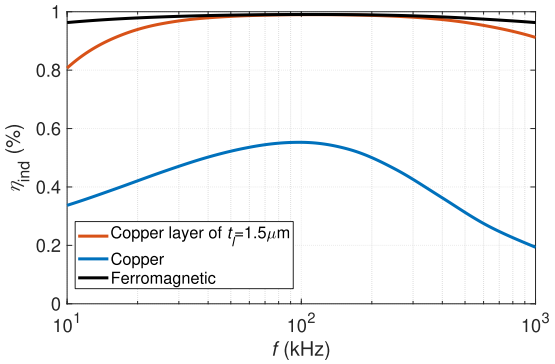

FIGURE 4. Simulated induction efficiency with respect to the frequency for different cases of load and materials.

ferrite thickness $t_f = 3.5$ mm. This winding has the same mean radius of the single turn of the analytical analysis and it consists of $n = 25$ turns. Windings are made of a litz wire of $n_s = 30$ strands of diameter $\phi_s = 0.2$ mm. Three different loads are tested, a copper layer of thickness $t_l = 1.5$ μm, and bulk copper and ferromagnetic disks of thickness $t_l = 5$ mm. The properties of materials are the same of those considered in the previous section, except the relative permeability of the flux concentrator, whose considered value is $\mu_r = 100$.

The induction efficiency with respect to the excitation frequency is simulated and the results are shown in Fig. 4. As it can be observed, the efficiency with the copper layer is similar to the achieved with a typical ferromagnetic material, and clearly higher than the efficiency of a copper pot. Moreover, in contrast with the flat characteristic of the efficiency observed for the ferromagnetic material, the efficiency for the layer deteriorates at frequencies lower than 30 kHz, which could be a practical limitation in the case of frequency-based power control. Apart from electromagnetic analysis, thermal or mechanical analysis have been not conducted in this work.

IV. EXPERIMENTAL VERIFICATION

Two different tests are conducted in order to check the proposal of this work. The first one is intended to verify the analytical and FEA modeling, and it is carried out by means of a set of samples of different layer thicknesses. The second is a proof of concept consisting of heating a glass pot with a deposited thin copper layer.

Regarding the set of samples, they were built on vitroceramic glasses of dimensions 120 × 120 × 2.5 mm. The results here presented are focused on samples of copper. The thickness of layers varies from 100 nm to 5 μm. Layers were deposited by means of the electron-beam phase vapor deposition (EBPVD) technique. This technique requires high vacuum atmosphere and it basically consists of sputtering atoms extracted from a bulk material with an electron beam into a target [32]. The EBPVD enables to deposit thin films with controlled thickness and texture, and allows the electrical conductivity of bulk materials to be practically preserved. This technique is used in different applications as optics, decorative architecture and magnetic recording, among others. The list of thicknesses is: 100 nm, 200 nm, 500 nm, 1 μm, 2 μm, and 5 μm. An image of a sample is shown in Fig. 5.

A flat spiral winding of $n = 23$ turns, with internal and external radii $r_{\text{int}} = 10$ mm, $r_{\text{int}} = 42.5$ mm, respectively was built for testing purposes. A fine magnet wire of diameter $\phi_s = 0.2$ mm was selected in order to minimize the frequency-dependent winding resistance contributions caused by the skin and proximity effects. As a consequence, the dc resistance of this inductor is very high and therefore it is not appropriate for heating purposes. However, the ac resistance of the winding is very small, or in other words, R_w can be considered as constant with respect to frequency, which is convenient for comparing measurements with the calculation results. A picture of the testing inductor is shown in Fig. 5b.

The equivalent impedance of the coil is measured with the Agilent E4980A LCR meter, which means that measurements correspond to small signal conditions and therefore thermal effects are not present. The frequency of measurements ranges from 10 kHz to 1 MHz. Calculated and experimental results are compared in Fig. 6. The results with conventional bulk copper and ferromagnetic pots are also presented for comparison purposes. It is observed that for thicknesses ranging from $t_l = 500$ nm to $t_l = 5$ μm the load resistances at the interest frequency range are higher than those obtained with the conventional ferromagnetic materials and, evidently, higher than the resistance obtained with the copper in bulk.

As it can be observed, the agreement between calculations and measurements is in general good. However, it should be noted that the conductivity of the bulk copper is not strictly preserved with the EBPVD technique. Nevertheless, for each thickness a conductivity allowing the observed agreement is found. These conductivities range from 2.25×10^7 $(\Omega\text{m})^{-1}$ for the layer of $t_l = 100$ nm to 5.3×10^7 $(\Omega\text{m})^{-1}$ for the layer of $t_l = 5$ μm, whereas the conductivity of the bulk copper is $\sigma_{\text{Cu}} = 5.8 \times 10^7$ $(\Omega\text{m})^{-1}$. These conductivities approximately follow a linear tendency with respect to the thickness (in log scale), as it is shown in Fig. 7. As it can be observed, the conductivity of the copper layer of $t_l = 100$ nm is approximately the half part of the conductivity of the bulk copper.

V. PROOF OF CONCEPT

A commercial Pyrex™ borosilicate glass pot is chosen for testing the concept here presented. The thickness of this glassware is 5 mm and its bottom radius is 65 mm. The thermal conductivity of the borosilicate glass is 1.15 $\left(\text{W}/\text{mK}\right)$, and the electrical conductivity is 1×10^{-9} $(\Omega\text{m})^{-1}$. Two different configurations are tested: first, a copper layer of thickness $t_l = 1.5\mu$m placed on the bottom (i.e in the inner part) of the glass pot (hereinafter called up layer); second, a copper layer of thickness $t_l = 2\mu$m placed at the bottom of the glass pot, and hereinafter called down layer. In the first configuration the heat source is in contact with the water but the distance between the inductor and the layer is higher than in the second case. Moreover, a conventional ferromagnetic pot (whose

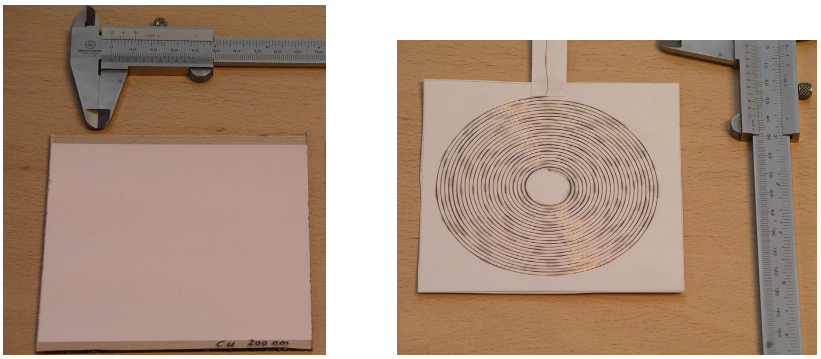

(a) (b)

FIGURE 5. (a) Image of a sample with a layer of $t_l = 200$ nm of copper. (b) Testing inductor.

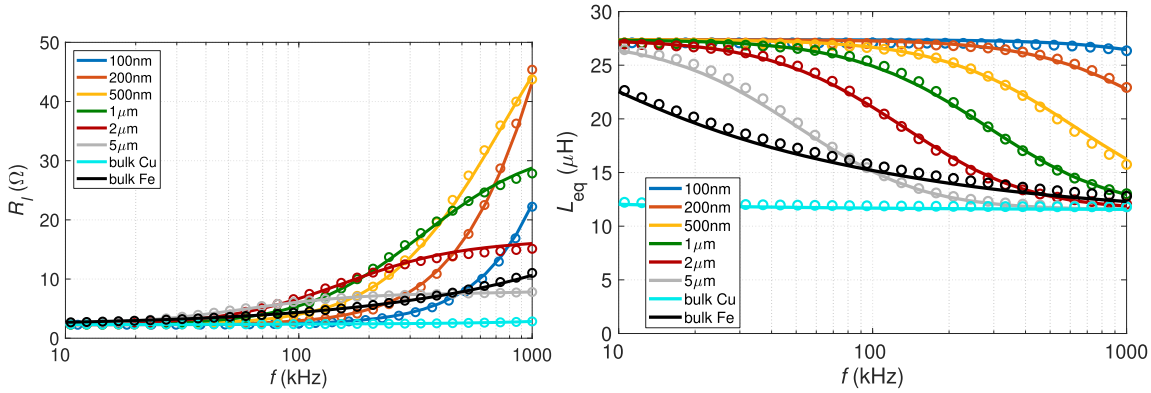

(a) (b)

FIGURE 6. Comparison between theoretical and experimental results for the thin layer samples, bulk and ferromagnetic materials. (a) Load contribution resistance. (b) Equivalent inductance.

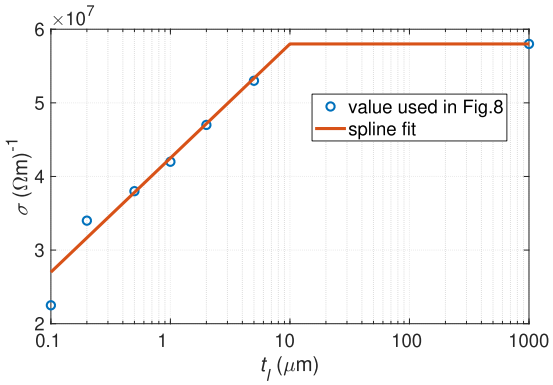

FIGURE 7. Conductivity of the samples with respect to the thickness of the layer and spline fit.

properties are assumed to be equal to those presented in Section I) is also tested for comparison purposes.

Prototypes are checked at high signal level conditions by means of an inductor of $P_o = 1.5$ kW of rated power. The external and internal radii of the inductor are $r_{\text{ext}} = 55$ mm, and $r_{\text{int}} = 20$ mm, respectively. Consequently, the inductor is completely covered by the glass pot. The inductor comprises $n = 26$ turns of a copper litz wire of $n_s = 30$ strands of diameter $\phi_s = 0.2$ mm. Pictures of the glass pot with the layer and the inductor are shown in Fig. 8. A ferrite plane made of Ferroxcube 3C90 ferrite bars placed below the inductor and an aluminum sheet are also included in the system.

The first tests are focused on checking the correctness of the model when both the pot and the inductor of Fig. 8 are considered. Therefore, impedance is measured by means of the LCR meter and results are compared with simulations in Fig. 9.

Moreover, induction efficiency of the three tested loads are shown in Fig. 10. As it is shown, the efficiency is similar for the three cases in the range comprised between 40 kHz and 100 kHz, although the down layer pot shows a slightly higher efficiency than the others. For the frequencies ranging from 20 kHz to 40 kHz, the efficiency of the up layer pot is clearly lower than the others. However, it is necessary to note that the electromagnetic conditions are not equal for the three loads because in the case of the up layer pot the distance from the windings to the metallic material doubles the other cases and, according to (2), the resistance R_l exponentially decreases with the distance between windings and dissipative media.

The experimental setup also includes a conventional series-resonant half-bridge inverter whose dc voltage is supplied by a full bridge rectifier connected to the mains. In this applications, where a high ripple of the dc bus is compatible

(a) (b)

FIGURE 8. (a) Glass pot with the down copper layer of $t_f = 2$ μm. (b) Testing inductor for high-level signal experiments.

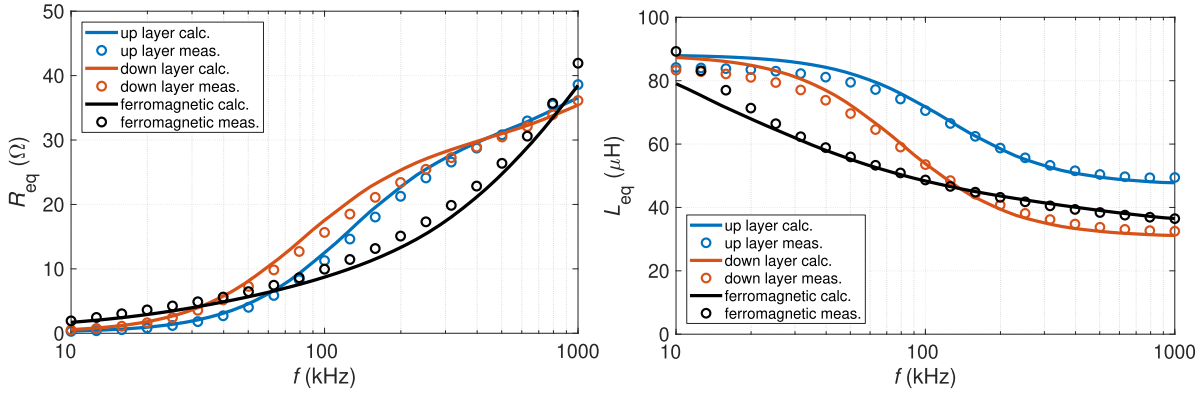

(a) (b)

FIGURE 9. Measured and simulated equivalent impedance at low signal level.

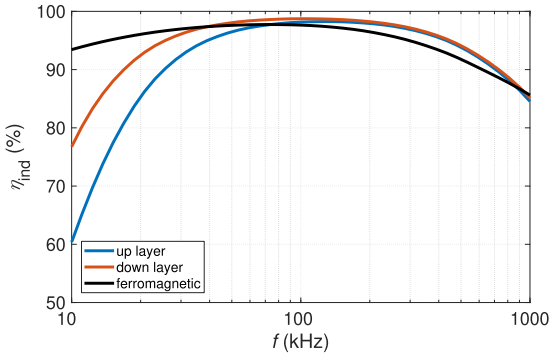

FIGURE 10. Simulated efficiency for the considered loads.

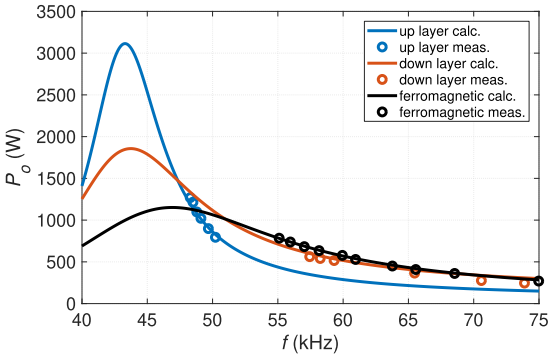

FIGURE 11. Calculated and experimental output power for the considered loads.

with operating specifications (i.e. cooking results), the output capacitor of the rectifier can be very small in order to achieve a power factor close to one. The series resonant capacitor value is $C_r = 156$ nF and it consists of the parallel of four capacitors of 39 nF. The resonant frequency with this resonant capacitor is about $f_r = 45$ kHz. Considering the harmonic analysis of this resonant circuit, the output power of the converter is

$$P_o = \sum_{h=1}^{\infty} \frac{2R_{\text{eq}}}{h^2\pi^2} \frac{V_{\text{m,rms}}^2}{\left[R_{\text{eq}}^2 + \left(h\omega_s L_{\text{eq}} - \frac{1}{h\omega_s C_r}\right)^2\right]} \quad \text{with} \quad h \text{ odd} \tag{10}$$

where h is the harmonic order, ω_s is the angular frequency corresponding to the switching frequency f_s, and $V_{\text{m,rms}}$ is the rms value of the mains voltage. According to the previous simulation results, both R_{eq} and L_{eq} depend on frequency. The power is also experimentally estimated by postprocessing the voltage and current captured with the Teledyne LeCroy HDO4054A digital oscilloscope. Therefore, calculated and measured output power with respect to frequency can be also compared as it is shown in Fig. 11.

The tested frequency range for each load is different and therefore a wider frequency span is covered. A boiling water

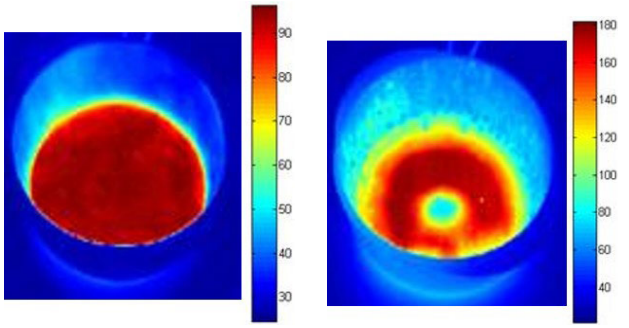

FIGURE 12. Thermal images of the up layer glass pot. (a) With water. (b) Without water.

regime for the glass pot with the up layer at $P_o = 1.25$ kW was reached. In this case the copper layer is cooled by the water and, therefore, its temperature is bounded and the testing supplied power can be higher. However, for the case of the down layer, the maximum supplied power is about $P_o = 500$ W in order to avoid dangerous high temperature for the layer. In general, the concordance between the measured power and simulated results is good.

Finally, thermal images are presented for the up layer glass pot in two cases, with and without water. These images are shown in Fig. 12. For the water-filled condition, the temperature is uniform and bounded by 100 °C). However, in the other case, higher temperature is reached and the temperature profile follows the typical power pattern generated by a spiral inductor with equally-spaced turns.

VI. CONCLUSION

The suitability of non-magnetic metallic thin layers for arranging induction heating cookware is explored in this work, with promising results. The induction efficiency is used as figure of merit for evaluating the cookware performance when the inductor and geometry are fixed. This parameter is evaluated in terms of resistances, which are obtained by means of an analytical model or FEA simulations. Calculations show that induction efficiencies higher than those achieved with conventional ferromagnetic pots can be achieved by using metallic layers with a specific thickness. For the case of copper, this thickness ranges from 1 μm to 2 μm. Moreover, it is also concluded that the optimum thickness is different at each frequency. The calculated results are checked by means of several prototypes with different arrangements, which are tested in real operating conditions. Experimental results shows good agreement with calculations. Finally, the results here presented open the possibility of manufacturing a new range of induction heating cookware from non-suitable materials as glass, ceramics or wood.

REFERENCES

[1] J. Acero, J. Burdío, L. Barragán, D. Navarro, R. Alonso, J. García, F. Monterde, P. Hernández, and S. L. I. Garde, "Domestic induction appliances," *IEEE Ind. Appl. Mag.*, vol. 16, no. 2, pp. 39–47, Mar. 2010.

[2] M. Perez-Tarragona, H. Sarnago, O. Lucia, and J. M. Burdio, "Design and experimental analysis of PFC rectifiers for domestic induction heating applications," *IEEE Trans. Power Electron.*, vol. 33, no. 8, pp. 6582–6594, Aug. 2018.

[3] S. Komeda and H. Fujita, "A phase-shift-controlled direct AC-to-AC converter for induction heaters," *IEEE Trans. Power Electron.*, vol. 33, no. 5, pp. 4115–4124, May 2018.

[4] H. Sarnago, O. Lucia, and J. M. Burdio, "Interleaved resonant boost inverter featuring SiC module for high-performance induction heating," *IEEE Trans. Power Electron.*, vol. 32, no. 2, pp. 1018–1029, Feb. 2017.

[5] C. Bi, H. Lu, K. Jia, J.-G. Hu, and H. Li, "A novel multiple-frequency resonant inverter for induction heating applications," *IEEE Trans. Power Electron.*, to be published.

[6] H.-P. Park and J.-H. Jung, "Load-adaptive modulation of a series-resonant inverter for all-metal induction heating applications," *IEEE Trans. Ind. Electron.*, vol. 65, no. 9, pp. 6983–6993, Sep. 2018.

[7] A. Dominguez, L. A. Barragan, J. I. Artigas, A. Otin, I. Urriza, and D. Navarro, "Reduced-order models of series resonant inverters in induction heating applications," *IEEE Trans. Power Electron.*, vol. 32, no. 3, pp. 2300–2311, Mar. 2017.

[8] V. Esteve, J. Jordan, E. Sanchis-Kilders, E. J. Dede, E. Maset, J. B. Ejea, and A. Ferreres, "Enhanced pulse-density-modulated power control for high-frequency induction heating inverters," *IEEE Trans. Ind. Electron.*, vol. 62, no. 11, pp. 6905–6914, Nov. 2015.

[9] J. Serrano, J. Acero, I. Lope, C. Carretero, and J. M. Burdio, "A flexible cooking zone composed of partially overlapped inductors," *IEEE Trans. Ind. Electron.*, vol. 65, no. 10, pp. 7762–7771, Oct. 2018.

[10] J. Serrano, I. Lope, J. Acero, C. Carretero, J. M. Burdio, and R. Alonso, "Design and optimization of small inductors on extra-thin PCB for flexible cooking surfaces," *IEEE Trans. Ind. Appl.*, vol. 53, no. 1, pp. 371–379, Jan. 2017.

[11] W. Han, K. T. Chau, and Z. Zhang, "Flexible induction heating using magnetic resonant coupling," *IEEE Trans. Ind. Electron.*, vol. 64, no. 3, pp. 1982–1992, Mar. 2017.

[12] I. Lope, J. Acero, and C. Carretero, "Analysis and optimization of the efficiency of induction heating applications with litz-wire planar and solenoidal coils," *IEEE Trans. Power Electron.*, vol. 31, no. 7, pp. 5089–5101, Jul. 2016.

[13] I. Lope, J. Acero, J. M. Burdio, C. Carretero, and R. Alonso, "Design and implementation of PCB inductors with litz-wire structure for conventional-size large-signal domestic induction heating applications," *IEEE Trans. Ind. Appl.*, vol. 51, no. 3, pp. 2434–2442, May 2015.

[14] F. Sanz, C. Sagues, and S. Llorente, "Induction heating appliance with a mobile double-coil inductor," *IEEE Trans. Ind. Appl.*, vol. 51, no. 3, pp. 1945–1952, May 2015.

[15] J. Acero, C. Carretero, R. Alonso, and J. M. Burdio, "Quantitative evaluation of induction efficiency in domestic induction heating applications," *IEEE Trans. Magn.*, vol. 49, no. 4, pp. 1382–1389, Apr. 2013.

[16] W. Han, K. T. Chau, C. Jiang, and W. Liu, "All-metal domestic induction heating using single-frequency double-layer coils," *IEEE Trans. Magn.*, vol. 54, no. 11, pp. 1–5, Nov. 2018.

[17] J. Acero, I. Lope, J. M. Burdio, C. Carretero, and R. Alonso, "Performance evaluation of graphite thin slabs for induction heating domestic applications," *IEEE Trans. Ind. Appl.*, vol. 51, no. 3, pp. 2398–2404, May 2015.

[18] P. Bergstrom and M. Trombley, "Induction heating of thin films," U.S. Patent 6 878 909 B2, Apr. 12, 2005.

[19] J. Acero, R. Alonso, J. Burdío, F. Villuendas, and L. Barragán, "Controlled-resistance loads for induction heating applications using thin non-magnetic metallic layers," *Electron. Lett.*, vol. 43, no. 8, p. 461, 2007.

[20] J. Acero, C. Carretero, R. Alonso, and J. M. Burdio, "Design of efficient loads for domestic induction heating applications by means of non-magnetic thin metallic layers," in *Proc. IEEE Appl. Power Electron. Conf. Expo. (APEC)*, Mar. 2016, pp. 3026–3031.

[21] C. Carretero, J. Acero, R. Alonso, and J. M. Burdio, "Normal-mode decomposition of surface power distribution in multiple-coil induction heating systems," *IEEE Trans. Magn.*, vol. 52, no. 2, pp. 1–8, Feb. 2016.

[22] K. Li, G. Y. Tian, L. Cheng, A. Yin, W. Cao, and S. Crichton, "State detection of bond wires in IGBT modules using eddy current pulsed thermography," *IEEE Trans. Power Electron.*, vol. 29, no. 9, pp. 5000–5009, Sep. 2014.

[23] A. Roskopf, E. Bar, C. Joffe, and C. Bonse, "Calculation of power losses in Litz wire systems by coupling FEM and PEEC method," *IEEE Trans. Power Electron.*, vol. 31, no. 9, pp. 6442–6449, Sep. 2016.

[24] M. Guarnieri, S. Lupi, and A. Stella, "Automatic design of axisymmetric induction heating systems," *IEEE Trans. Magn.*, vol. MAG-22, no. 5, pp. 822–824, Sep. 1986.
[25] C. Carretero, R. Alonso, J. Acero, and J. M. Burdio, "Coupling impedance between planar coils inside a layered media," *Prog. Electromagn. Res.*, vol. 112, pp. 381–396, 2011.
[26] C. Dodd, J. Luquire, W. Deeds, and W. Spoeri, "Some eddy current problems and their integral solutions," Oak Ridge Nat. Lab., Oak Ridge, TN, USA, Tech. Rep. W-7505-eng-26, Apr. 1969.
[27] W. Hurley and J. Kassakian, "Induction heating of circular ferromagnetic plates," *IEEE Trans. Magn.*, vol. MAG-15, no. 4, pp. 1174–1181, Jul. 1979.
[28] J. Acero, R. Alonso, L. Barragan, and J. Burdio, "Modeling of planar spiral inductors between two multilayer media for induction heating applications," *IEEE Trans. Magn.*, vol. 42, no. 11, pp. 3719–3729, Nov. 2006.
[29] J. Acero, R. Alonso, J. M. Burdio, L. A. Barragan, and D. Puyal, "Frequency-dependent resistance in Litz-wire planar windings for domestic induction heating appliances," *IEEE Trans. Power Electron.*, vol. 21, no. 4, pp. 856–866, Jul. 2006.
[30] C. Carretero, J. Acero, and R. Alonso, "TM-TE decomposition of power losses in multi-stranded Litz-wires used in electronic devices," *Prog. Electromagn. Res.*, vol. 123, pp. 83–103, 2012.
[31] C. Sullivan, "Cost-constrained selection of strand diameter and number in a Litz-wire transformer winding," *IEEE Trans. Power Electron.*, vol. 16, no. 2, pp. 281–288, Mar. 2001.
[32] H. K. Pulker, *Coatings Glass*. Amsterdam, The Netherlands: Elsevier, 1999.

J. ACERO (Member, IEEE) received the M.Sc. and Ph.D. degrees in electrical engineering from the University of Zaragoza, Zaragoza, Spain, in 1992 and 2005, respectively. From 1992 to 2000, he worked in several industry projects, especially focused on custom power supplies for research laboratories. Since 2000, he has been with the Department of Electronic Engineering and Communications, University of Zaragoza, where he is currently a Professor. His main research interests include resonant converters for induction heating applications, inductive-type load modeling, and electromagnetic modeling. Dr. Acero a member of the IEEE Power Electronics, Industrial Electronics and Magnetics Societies. He is also a member of the Instituto de Investigación en Ingeniería de Aragón (I3A).

I. LOPE (Member, IEEE) received the M.Sc. degree in electrical engineering and the Ph.D. degree in power electronics from the University of Zaragoza, Zaragoza, Spain, in 2010 and 2015, respectively. He is currently with the BSH Home Appliances, Zaragoza, where he is involved in several projects focusing on developing domestic induction heating appliances. His current research interests include electromagnetic modeling of inductive coupled contactless energy transfer systems and loss modeling of magnetic devices.

C. CARRETERO (Senior Member, IEEE) received the B.Sc. and M.Sc. degrees in physics, the B.Sc. and M.Sc. degrees in electrical engineering, and the Ph.D. degree in electrical engineering from the University of Zaragoza, Zaragoza, Spain, in 1998, 2002, and 2010, respectively. He is currently an Assistant Professor with the Department of Applied Physics, University of Zaragoza. His research interests include induction heating applications and electromagnetic modeling of inductive systems. He is a member of the Instituto de Investigación en Ingeniería de Aragón (I3A).

J. M. BURDIO (Senior Member, IEEE) received the M.Sc. and Ph.D. degrees in electrical engineering from the University of Zaragoza, Zaragoza, Spain, in 1991 and 1995, respectively.

In 2000, he was a Visiting Professor with the Center for Power Electronics Systems, Virginia Tech. He has been with the Department of Electronic Engineering and Communications, University of Zaragoza, where he is currently a Professor, the Head of the Group of Power Electronics and Microelectronics, and the Director of the BSH Power Electronics Laboratory, University of Zaragoza. He is the author of more than 80 international journal articles and over 200 articles in conference proceedings and the holder of more than 60 international patents. His main research interests include modeling of switching converters, and resonant power conversion for induction heating and biomedical applications. Dr. Burdio is a member of the Instituto de Investigación en Ingeniería de Aragón (I3A). He is also a Senior Member of the Power Electronics and Industrial Electronics Societies.